Assessment of Soil Strength
using a Robotically Deployed and Retrieved Penetrometer

Victor M. Baez[1], Ami Shah[1], Samuel Akinwande[1], Navid H. Jafari[2], and Aaron T. Becker[1]

Abstract— **This paper presents a method for performing free-fall penetrometer tests for soft soils using an instrumented dart deployed by a quadcopter. Tests were performed with three soil types and used to examine the effect of drop height on the penetration depth and the deceleration profile. Further tests analyzed the force required to remove a dart from the soil and the effect of pulling at different speeds and angles. The pull force of a consumer drone was measured, and tests were performed where a drone delivered and removed darts in soil representative of a wetland environment.**

I. INTRODUCTION

This study is part of an initiative to develop a robot to deploy and retrieve sensors that would enable coastal scientists to measure data at a larger spatial scale and finer temporal scale than current methods. This paper focuses on the design and test of a free-falling penetrometer shown in Fig. 1. UAV deployed and retrieved sensors could increase the spatial and temporal density of wetland soil measurements. By coupling these measurements to fine resolution hydrologic models, we will better understand the surface-subsurface hydrodynamic interactions that control the biological processes in wetland soils. The fundamental knowledge gained would enhance future wetland models [1]–[3]. Similar methods could enable in-situ tests to rapidly evaluate wetland soil properties, eliminating many drawbacks involved with field core sampling and decreasing the number of core samples required.

Wetland vulnerability is commonly assessed using a three-tiered framework of landscape-scale assessment, rapid assessment protocols, and intensive biological and physiochemical measurements. All three methods involve manually trekking through the wetlands to collect cores for evaluating substrate biological and physical properties (see Fig. 2). These laborious procedures are inefficient in terms of mobilizing equipment, productivity, paucity of data, and disturbance to the wetlands. Beyond the substantial time commitment required for analyzing field cores, measurement errors are pervasive due to variations in operation, type, and dimension of the coring device; compression of the sediment when taking the core and/or when extracting the core from the core tube; imprecise sectioning of the core into known volumes, variation in drying and furnace temperatures, and
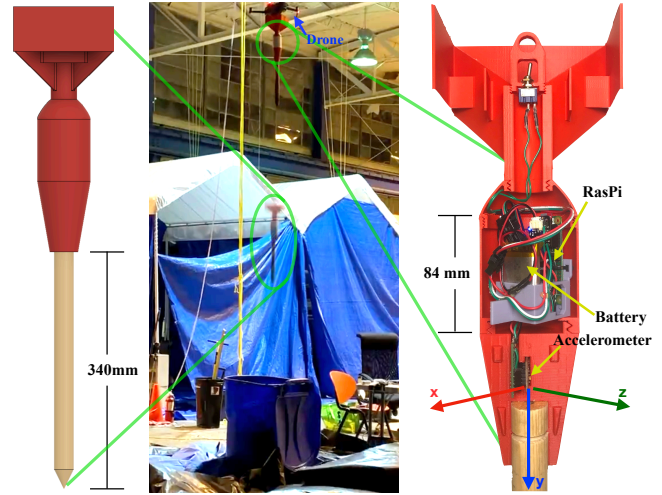

Fig. 1: The drone-delivered soil penetrometer. (left) Rendering of the dart. (center) Composite photograph of drone delivering a dart. (right) Physical cross-section showing the electronics package and components.

presence of salts that precipitate when the pore water is evaporated from the sample [2].

This study targets rapid assessment protocols and it also provides new knowledge to enhance the fundamental principles underlying landscape assessment models. Rapid assessments of wetland conditions use hydrology, hydric soils, and wetland biotic communities to understand changes in wetland function, ecological integrity, and mitigation success. However, the soil assessment components are the least developed [4]. Thus, the addition of wetland soil data will strengthen salt marsh assessments because soils provide a record of both long and short-term changes in wetland conditions as a result of anthropogenic effects such as tidal restriction. There is a need to develop soil indicators to guide the efficacy of restoration projects, e.g., rebuilding drowning marshes using dredged sediment, improving drainage, and facilitating marsh migration. This is especially important in the wake of Hurricanes Katrina, Sandy, and Harvey where investment in natural infrastructure has increased substantially. $20B of projects are planned in Louisiana over the next 50 years for marsh restoration, sediment diversions, and shoreline protection. For a video overview of this project, see `https://youtu.be/Kjes2r0Hjsw`.

II. RELATED WORK

Cone penetrometer testing is used in the field of geotechnical engineering to explore the subsurface stratigraphy and properties for the design of civil infrastructure [5]. The cone consists of a 0.1 m diameter rod with a conical tip that is

[1] Authors are with the Department of Electrical and Computer Engineering, University of Houston, Houston, TX 77204 USA {atbecker}@uh.edu
[2] Author is with the Department of Civil and Environmental Engineering, Louisiana State University, Baton Rouge, LA 70803 USA njafari@lsu.edu
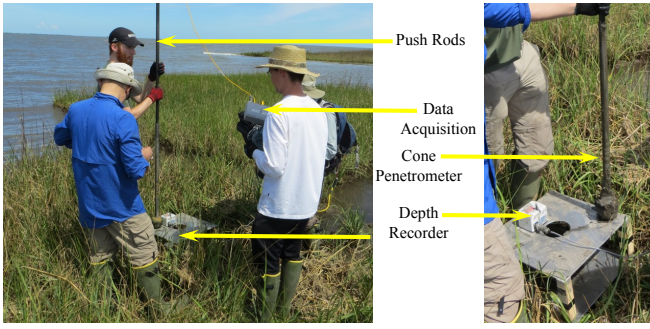
Fig. 2: Manually obtaining CPT data from a wetland requires multiple people, and trekking over sensitive wetlands. The method presented in this paper could reduce the impact on the wetlands, and both simplify the automate the testing procedure.

Fig. 3: The three soils used for the experiments. 0.125 cubic meters of each soil type was placed in three plastic bins for the drop experiments.

driven into the ground at a rate of 20 mm/s. As it penetrates into soil, it measures the tip and sleeve resistance, along with pore-water pressure. These three variables are used together to identify soil types and estimate engineering properties, such as shear strength, stress history, and stiffness. The output of CPTs are used to design foundations for buildings, bridges, dams, levees, and other infrastructure. They are used to estimate the probability of liquefaction of sands and tailings dams during earthquakes. Recent innovations of the CPT have involved applying the test to coastal and offshore environments. However, conducting CPTs in offshore environments is expensive because of the cost of mobilization in such extreme environments. The free fall penetrometer (FFP) was developed in response to explore seafloor sediment in the upper 10 m [6]. The FFP involved dropping a dart into the ocean such that it accelerates to a terminal velocity and hence approaches free fall. The FFP was instrumented with a series of accelerometers such that the deceleration of the dart is captured. The acceleration time history is double integrated to evaluate the depth of penetration into the seabed. The acceleration behavior was also used to estimate a quasi-static bearing capacity of the soil.

The dart developed in this study builds upon the FFP. However, penetrating subaerial soil presents different challenges than in submarine environments because offshore deposits (cohesive and sands) are typically loosely deposited and thus soft. Terrestrial soils can vary significantly in particle size, consistency stiffness, and inclusion of roots or vegetation. Therefore, penetrating these soils is difficult. Moreover, the ability of the dart to penetrate soils is a function of the velocity at impact, which is correspondingly a function of drop height. In this scenario, the complexity arises from ensuring the dart penetrates the soil vertically with sufficient velocity and developing a means for extracting the dart in the soil using the force capability of a UAV.

The concept of dropping a dart equipped with a sensitive accelerometer to measure soil properties is not new. Mulukutla et al. used a heavy dart-shaped sensor dropped into seawater to measure the soil properties of the ocean bed [7]. Naxem et al. employed these for analyszing the dynamics of falling into uniform clay [8]. Mumtaz and Stark investigated of pore pressures during high-velocity impact by a free fall penetrometer in [6], [9]. White et al. performed similar tests in sand to measure the equivalent static resistance [10], and Stark used these for near-shore zones [11].

There is also impressive research on using drone to take core samples [12], [13]. This is related to our priot work using drones to deploy seismic sensors [14]–[16], only in this work the sensing takes place during the deployment, and the darts can then immediately be retrieved and redeployed to a new area.

III. METHODOLOGY

A. The Free-falling penetrometer dart

We designed a 3D-printed dart that consists of a 400 g accelerometer (Sparkfun H3LIS331DL) and connected it to a Raspberry Pi Zero. Both are contained inside a ballistic projectile with a 340 mm wooden spike at one end and a stabilizer at the other. The Raspberry Pi and LiPo battery were placed so the center of mass was on the y-axis and the accelerometer is placed so the y-axis is aligned with the spike of the dart. This placement directs the impact force along the y-axis. Figure 1 shows the design.

B. The delivery vehicle

To deploy our FFP, we used a DJI Mavic Pro 2 equipped with an E-flight servoless payload release mechanism that was actuated using an RC controller. The stock Mavic 2 has a take-off weight of 907 grams, and a rated take-off weight of 1,100 grams.

C. Description of soils

Three soil were used to represent a range of soil types found in a wetland. The first was *torpedo sand*, a naturally occurring course-grained sand and gravel mix. The second soil was *beach volleyball sand*, which consists of at least 80% 0.5 mm - 1.0 mm particles. The third soil was saturated marsh mud. Figure 3 shows all three soils used for this study.

The water content of each soil was estimated by measuring the change in mass when of a container of soil was dried at 100°C for 48 hours in a laboratory furnace. The water content of the torpedo soil was 7.46%, the volleyball sand was 11.68%, and the saturated mud was 30.5%.

D. Procedure for drops and pull force experiments

We took two steps to ensure consistency between tests: (1) the soil was prepared to simulate virgin soil and (2) the drops were performed using a pulley system to ensure uniform height and loose starting conditions.

In between tests, the different soil types were prepared using a hand cultivator, shovel, and a garden claw. The combination of these tools were used to generate a uniform consistency of the soil mixture throughout the entire bin. To do accomplish this, we mixed the soil for a minimum of one minute and then leveled the soil. The dart was manually dropped using a pulley system. Penetration depth was measured from the tip of the dart to the highest part of the dart that was in contact with the soil.

E. Measuring pull forces for the dart and the drone

To measure pull forces with consistency, two setups were used. To measure the pull force required to remove a dart, a stepper motor actuated a one meter long linear stage (OpenBuildsPartStore.com C-Beam). The linear stage pulled a 1.5 mm steel cable, attached to an s-type load cell (10 kg, CALT) that was fixed to the tail end of the dart. Figure 4 shows the setup: the linear rail, the load cell, and the dart.

To measure the pull forces exerted by the drone, a rig was used to counterweight an s-type load cell (10 kg, CALT). The rig was constrained to rotate on one axis using ball-bearings. The drone was attached to the rig by a 1.5 mm diameter steel cable, as shown in Fig. 5.
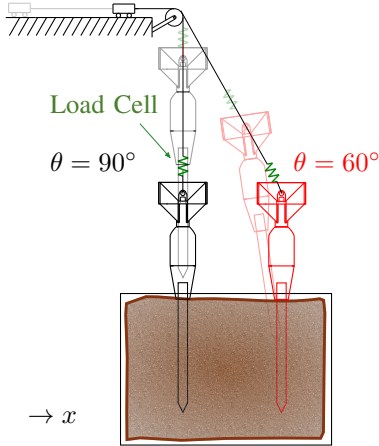

Fig. 4: Experimental setup for measuring the force required to pull a dart from soil. To make different pulling angles θ, the container of soil is shifted along the x-axis. Shown are $\theta = 90°$ and $\theta = 60°$. The strain gauge is at the tail of the dart, and a cable was run up to the linear actuator. The experiments vary the speed of the linear actuator and the angle of pulling.

IV. EXPERIMENTS

A. Varying altitude of dart drops and soil types

Our first experiment considers altitudes at which a drone must drop a FFP to distinguish soil types. To find suitable altitudes for our FFP to distinguish soil types, we recorded the deceleration of the impact event of our FFP into the three different soils from three different drop heights. The drop heights were measured as the distance from the tip of the spike to the top of the soil. The heights tested were 3.7m, 2.5m, and 1.5m, as shown in Fig. 6 and 7.
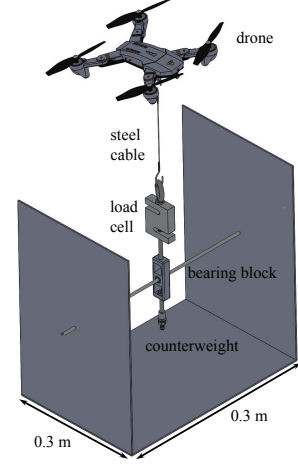

Fig. 5: Testing rig for measuring the pull force of a drone.

B. Measuring pull force required to extract a dart

The force required to extract a dropped dart varies with the pulling angle and the speed of pulling. For each pull test, after preparing the soil, the FFP was buried in the soil the total length of the spike (340 mm), and the soil was tamped flat. To vary the angle that we pulled the dart out of our mud, the pulley remained stationary, and the container of soil with the buried dart was moved horizontally, taking care to ensure the dart remained vertical. The pull angle was defined as the angle from horizontal of the cord that pulled the dart. This cord connected the tail of the dart to the linear stage.

For our fastest velocity, (333 mm/s), we used a power drill to rotate the threaded rod on the linear actuator. For 27.3 mm/s and 13.6 mm/s, the threaded rod was rotated using a stepper motor.

C. Measuring pull force of a drone

To measure the pull force of a drone, we ran three experiments. The first experiments measured the transient and steady state forces applied by the drone when pulling upwards (90°), using the testing rig shown in Fig. 5.

The next experiments measured the steady-state forces exerted by the drone when pulling at different angles (60°, 70°, 80°, 90°) from horizontal, also using the testing rig shown in Fig. 5.

The final experiments used the drone to retrieve an FFP that the drone had dropped into the soil. After each drop, a load cell was attached between the drone and the dart, and the pulling forces were recorded. In these tests, we documented the difference in pulling forces required to retrieve a bare dart with using a dart that had a sacrificial sleeve which was left behind. An illustration is shown in Fig 14.

V. RESULTS

Fig. 6 shows the impact deceleration for two sands and a cohesive mud. The acceleration starts at 0 until the dart is dropped from the specific height, after which it accelerates through the duration of the drop height. At this point, the dart impacts the soil, begins to penetrate the soil, and decelerates
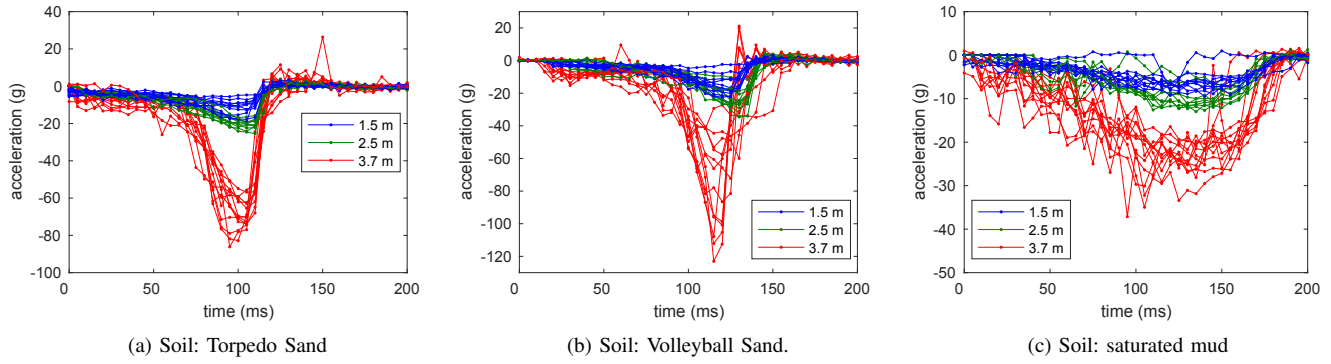
(a) Soil: Torpedo Sand   (b) Soil: Volleyball Sand.   (c) Soil: saturated mud

Fig. 6: Plot of the impact deceleration of our dart from three different drop heights into three soils.

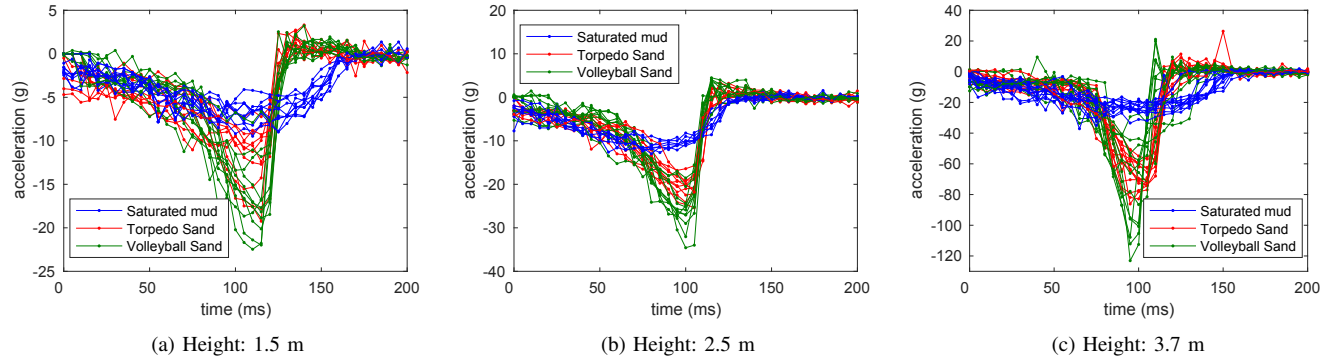(a) Height: 1.5 m   (b) Height: 2.5 m   (c) Height: 3.7 m

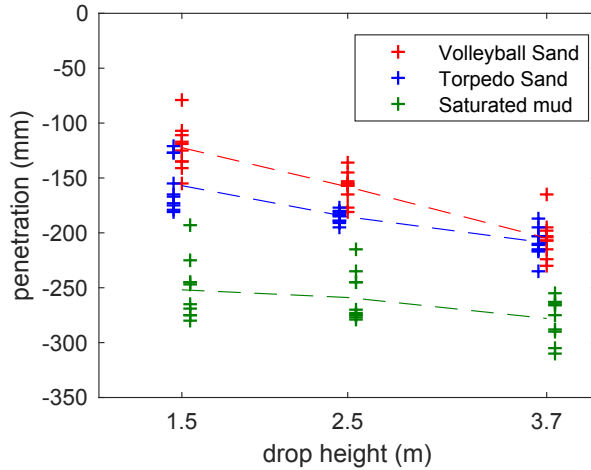Fig. 7: Distinguishing soil types using three different drop heights.

Fig. 8: Penetration Depth as a function of drop height and soil type. Penetration depth increases with drop height. The sands are similar, but the FFP penetrates roughly twice as deep into the saturated mud.
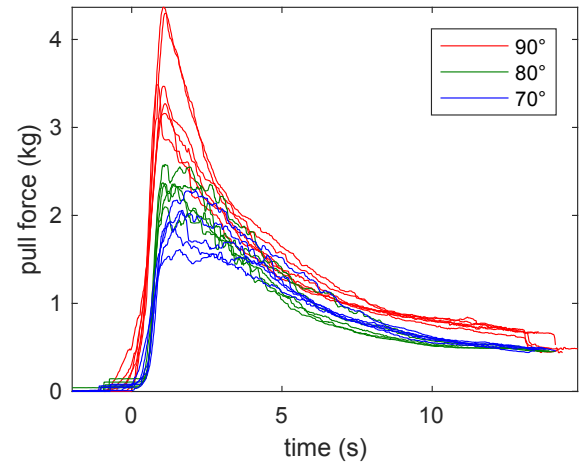
Fig. 9: Pulling darts from saturated mud at different angles from vertical. See Fig. 4 for definition of pull angle. All pulls were at 27.3 mm/s using a linear actuator, and the darts were buried 340 mm in the soil.

until it comes to a rest. The two sands in Fig. 6(a) and 6(b) show a sharp peak at approximately 100 g, while Fig. 6(c) shows a more shallow curve for the mud. In particular, the max acceleration experienced in the mud was 30 g. Sand is more stiff than clay so the behavior observed in Fig. 6 indicates that higher accelerations correspond to higher strength soils. The narrow area under the curve for the sands indicates the dart comes to a rest more rapidly than the mud. This further suggests that the dart penetrated less into the sands than mud. An observable difference in the acceleration time history was not evident until the highest drop, suggesting a

minimum drop height is needed for successful penetration. Between the experiments, visual inspection shows that there is reproducibility of the tests. More variability is found in Fig. 6(b) but the results are promising.

Fig. 7 shows the change in acceleration for each specific soil type but plotted with consistent drop height. For a drop height of 1.5 m, the acceleration in mud reaches 8 g, whereas the torpedo sand and volleyball sand approach 12 g and 20 g, respectively. When the drop height increases to 2.5 m, the mud still shows the same behavior with a slight increase to 10 g. The sands now overlap (volleyball sand
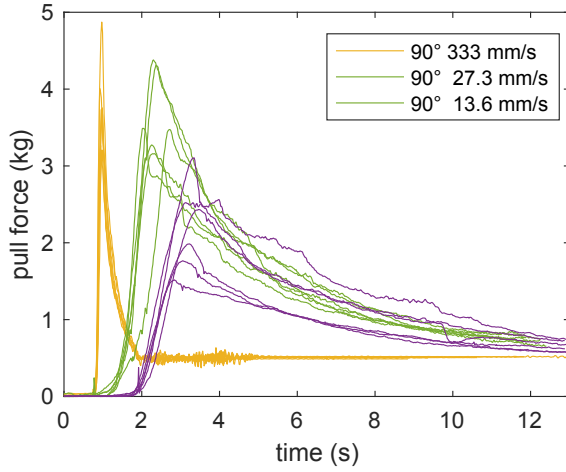
Fig. 10: Pulling darts from saturated mud at different speeds. Faster speeds increase the maximum pull force.

Fig. 12: The drone steady-state pull force is maximum at 90°, and has the least variation. Each error-bar shows the mean and standard deviation for a test for 7 seconds of steady-state pulling at the desired angle, measured visually with a large printed protractor using the testing rig shown in Fig. 5.
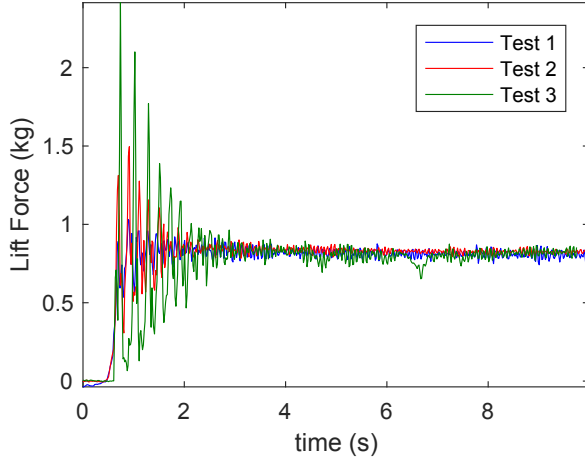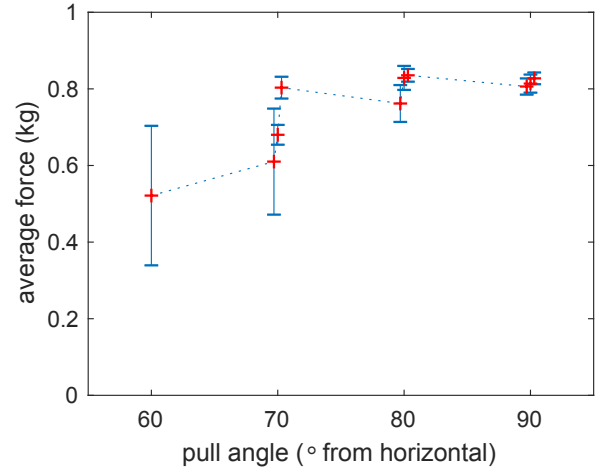

Fig. 11: Maximum drone lift at 90° during three trials pulling on a load cell using the testing rig shown in Fig. 5. After a 1 second transient, with force ranging up to 2.4 kg, the force stabilizes at 0.82 ± 0.02 kg.
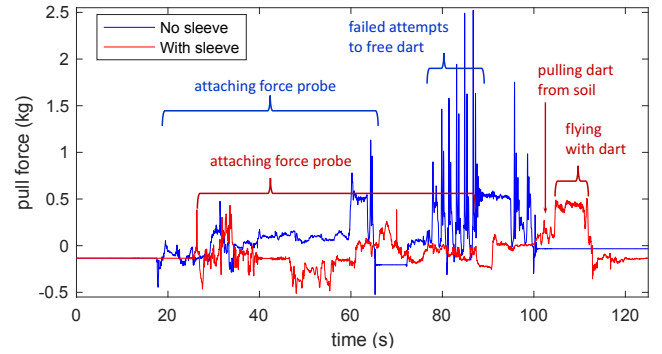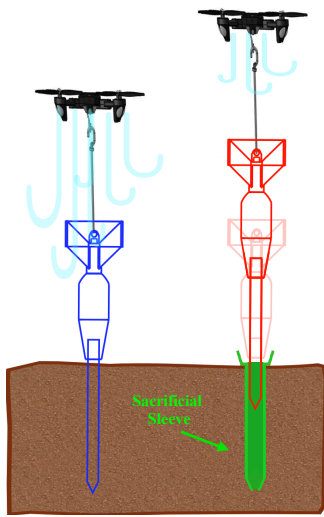

Fig. 13: After the drone dropped the FFP, a force probe was mounted between the drone and the dart to measure pulling forces. Three trials were performed using the bare FPP and three trials where the FFP was covered with a sacrificial sleeve. The small drone used in these experiments was unable to pull the bare FFP from the mud, but was successful each time with the sacrificial sleeve. This plot shows representative force data.

is slightly higher at 25 g compared to 20 g for torpedo sand) and suggest similar behavior and stiffness. The highest drop height of 3.7 m indicates a mud acceleration is 20 g and the torpedo sand approaches 80 g. The volleyball sand is evidently stiffer than the rest of the soils. This is further evident in Fig. 8, which shows the penetration depth. In particular, the mean penetration depth was 110 mm and 160 mm for volleyball sand and torpedo sand, respectively, for a drop height of 1.5 m. For the sands, the penetration depth increases linearly with increasing drop height to 3.7 m. In contrast, the penetration depth for mud remains more constant over the drop heights.

Fig. 9 shows the pull force necessary to retrieve the dart. The tests were completed at three different angles of 70°, 80°, and 90°. The highest pull force of 3.5 kg corresponds to 90°, while 70° pull force is lower at approximately 2 kg. In other words, the required pull-out force is higher by a factor of 1.75 with 90° compared to 70°. The reason for this behavior is twofold. The 90° test is located directly under the pulley while the 70° shifts to the right. A moment is exerted

when pulling commences. Also, the rotation of the dart at 70° breaks the adhesion of the mud to the dart. This makes it easier to pull the dart out. The lateral restraint (bearing capacity) of the mud is also less than vertical suction as the dart rotates.

In Fig. 10, the pull-out force was measured as a function of velocity at a constant angle of 90°. As the speed increases, the pull-out force also increases. For example, a pull-out force of approximately 2 kg is necessary at 13.6 mm/s, 3.5 kg for 27.3 mm/s, and 4 kg at 333 mm/s. The increase in pull force is attributed to the viscoelastic behavior of soils, where increasing strain rate increases the strength of the soil. As a result, the increasing speeds correspond to increased strain rates and the pull-out force is concomitantly increasing.

Figure 11 shows the forces exerted by a manually-piloted drone pulling upwards (90°). In each of the three trials, the forces exhibit an oscillatory transient that dies out after approximately 1 second. This transient behavior consists of a range of values that peak at 2.4 kg. The steady state force is uniform, stabilizing to 0.82 ± 0.02 kg. This indicates that the

14: Technique for retrieval of a drone-deployed FFP using a sleeve that is left behind.

maximum lift force from the drone is insufficient compared to the required pull force in Figs. 9 and 10.

Figure 9 shows that the force required to retrieve a dart decreases when the dart is pulled at lower angles. However, as Fig. 12 shows, the maximum drone pulling force also decreases with angle. Ten trials are shown at four different angles, all manually piloted. The force at $60°$ is 0.52 ± 0.18 kg, at $70°$ is 0.70 ± 0.06 kg, at $80°$ is 0.81 ± 0.03 kg, and at $90°$ is 0.82 ± 0.02 kg.

The maximum pulling force the drone can exert is less than the force required to free the dart in Fig. 9. Field tests will require a drone with a larger pulling force. We ran three trials where the drone dropped the dart from a height of approximately 2.5 m into the saturated mud soil and then attempted to retrieve the dart. We inserted a load cell between the drone and the dart and recorded the pull force. Fig. 13 shows the forces exerted as the drone attempted to retrieve the dart with and without a sacrificial sleeve. Trials using a 3D-printed sacrificial sleeve on the dart enabled successful retrieval. The sacrificial sleeve was made of PLA and designed to fit the spike of the dart, with a wall thickness of 2 mm, and used a thin foam gasket between the top of the spike and the dart body to prevent the sleeve from jamming onto the spike. Future implementations could use a servo to release the sleeve, but in these trials a thin strip of duct tape was used to secure the sleeve to the dart during the deployment, and manually removed before retrieval.

VI. CONCLUSION

Innovative technology that leverages robotics can provide a significant step forward in quantifying how coastal ecosystems change with environmental stressors. In particular, there is an important need to make field measurements more frequent at a large spatial region. This paper presents a method for performing free-fall penetrometer tests for sand and mud soils using an instrumented dart deployed by a quadcopter. The experimental program included quantifying the deceleration profile and penetration depth at various drop heights. Less penetration was observed in the sand compared to mud, which is a surrogate for soil strength. Further,

tests performed to estimate the pull-out force required to retrieve the dart indicate the force is less at lower angles but more at higher speeds. The pull force of a consumer drone was measured to be approximately 0.8 kg, and tests were performed where a drone delivered and removed darts in soil representative of a wetland environment. This study showed that a UAV-deployable FFP can provide insights into soil properties, but considerable challenges remain.

REFERENCES

[1] D. L. Passeri, S. C. Hagen, S. C. Medeiros, M. V. Bilskie, K. Alizad, and D. Wang, "The dynamic effects of sea level rise on low-gradient coastal landscapes: A review," *Earth's Future*, vol. 3, no. 6, pp. 159–181, 2015.

[2] J. T. Morris, D. C. Barber, J. C. Callaway, R. Chambers, S. C. Hagen, C. S. Hopkinson, B. J. Johnson, P. Megonigal, S. C. Neubauer, T. Troxler *et al.*, "Contributions of organic and inorganic matter to sediment volume and accretion in tidal wetlands at steady state," *Earth's future*, vol. 4, no. 4, pp. 110–121, 2016.

[3] K. Alizad, S. C. Hagen, J. T. Morris, P. Bacopoulos, M. V. Bilskie, J. F. Weishampel, and S. C. Medeiros, "A coupled, two-dimensional hydrodynamic-marsh model with biological feedback," *Ecological Modelling*, vol. 327, pp. 29–43, 2016.

[4] T. M. Twohig and M. H. Stolt, "Soils-based rapid assessment for quantifying changes in salt marsh condition as a result of hydrologic alteration," *Wetlands*, vol. 31, no. 5, p. 955, 2011.

[5] P. Robertson and K. Cabal, *Guide to Cone Penetration Testing For Geotechnical Engineering*, 6th ed. Signal Hill, California: Gregg Drilling & Testing, Inc., 2015.

[6] M. Mumtaz, N. Stark, and S. Brizzolara, "Pore pressure measurements using a portable free fall penetrometer," in *Cone Penetration Testing 2018: Proceedings of the 4th International Symposium on Cone Penetration Testing (CPT'18), 21-22 June, 2018, Delft, The Netherlands*. CRC Press, 2018, p. 461.

[7] G. K. Mulukutla, L. C. Huff, J. S. Melton, K. C. Baldwin, and L. A. Mayer, "Sediment identification using free fall penetrometer acceleration-time histories," *Marine Geophysical Research*, vol. 32, no. 3, pp. 397–411, 2011.

[8] M. Nazem, J. P. Carter, D. W. Airey, and S. Chow, "Dynamic analysis of a smooth penetrometer free-falling into uniform clay," *Géotechnique*, vol. 62, no. 10, pp. 893–905, 2012.

[9] M. B. Mumtaz, "Investigation of pore pressures during high-velocity impact by a free fall penetrometer," Ph.D. dissertation, Virginia Tech, 2018.

[10] D. White, C. O'Loughlin, N. Stark, and S. H. Chow, "Free fall penetrometer tests in sand: Determining the equivalent static resistance," in *Cone penetration testing 2018: Proceedings of the 4th international symposium on cone penetration testing*. CRC Press Boca Raton, FL, USA, 2018, pp. 695–701.

[11] N. Stark, B. Radosavljevic, B. Quinn, and H. Lantuit, "Application of portable free-fall penetrometer for geotechnical investigation of arctic nearshore zone," *Canadian Geotechnical Journal*, vol. 54, no. 1, pp. 31–46, 2017.

[12] Y. Sun, A. Plowcha, M. Nail, S. Elbaum, B. Terry, and C. Detweiler, "Unmanned aerial auger for underground sensor installation," in *2018 IEEE/RSJ International Conference on Intelligent Robots and Systems (IROS)*. IEEE, 2018, pp. 1374–1381.

[13] A. Plowcha, Y. Sun, C. Detweiler, and J. Bradley, "Predicting digging success for unmanned aircraft system sensor emplacement," in *International Symposium on Experimental Robotics*. Springer, 2018, pp. 153–164.

[14] S. K. Sudarshan, L. Huang, C. Li, R. Stewart, and A. T. Becker, "Seismic surveying with drone-mounted geophones," in *2016 IEEE International Conference on Automation Science and Engineering (CASE)*. IEEE, 2016, pp. 1354–1359.

[15] R. Stewart, L. Chang, S. Sudarshan, A. Becker, and L. Huang, "An unmanned aerial vehicle with vibration sensing ability (seismic drone)," in *SEG Technical Program Expanded Abstracts 2016*. Society of Exploration Geophysicists, 2016, pp. 225–229.

[16] S. K. Sudarshan, V. Montano, A. Nguyen, M. McClimans, L. Chang, R. R. Stewart, and A. T. Becker, "A heterogeneous robotics team for large-scale seismic sensing," *IEEE Robotics and Automation Letters*, vol. 2, no. 3, pp. 1328–1335, 2017.